

Trends in transmission and mortality rates of the Covid-19 pandemic estimated from publicly available data

John Sibert*

Joint Institute of Marine and Atmospheric Research
University of Hawai‘i at Mānoa
Honolulu, HI 96822 U.S.A.

August 10, 2020

Abstract

A simple compartment model of Covid-19 infections and deaths is applied to publicly available data. The model estimates trends and transmission and mortality rates using random effects. Model estimates of infections and deaths match observations closely. Trends in estimated transmission rate vary substantially between geographic areas. Transmission rates were suppressed below 0.007da^{-1} by the end of May in some areas, but rebounded when social constraints were relaxed in other areas. Mortality rates of individuals infected with Covid-19 fell to less than 0.001da^{-1} in most areas by the end of July. These results show that publicly available data, often collected and compiled with different protocols, can be used to quantitatively estimate trends in transmission and mortality rate.

*sibert@hawaii.edu; johnrsibert@gmail.com

Introduction

The sudden advent of the Covid-19 pandemic provoked many political jurisdictions to advise people to “shelter in place” and to practice “social distancing”. If this advice has been effective, it should be possible to detect the effects of the advice by comparing changes in transmission rates over time and between areas. SIR models are often applied to the spread of epidemics and have certainly been applied to the current Covid-19 pandemic (e.g. Chen et al. 2020; Roques et al. 2020). These models divide the affected population into three compartments: susceptible (S), Infected (I) and Recovered (R). SIR models are usually expressed as coupled ordinary differential equations,

$$\frac{dS}{dt} = -\beta \frac{IS}{N} - \mu S \quad (1)$$

$$\frac{dI}{dt} = \beta \frac{IS}{N} - \mu I - \gamma I \quad (2)$$

$$\frac{dR}{dt} = -\mu R + \gamma I \quad (3)$$

$$N = S + I + R \quad (4)$$

where N is the population size, β is the instantaneous transmission rate ($[t^{-1}]$), μ is the instantaneous mortality rate ($[t^{-1}]$), and γ is the instantaneous recovery rate ($[t^{-1}]$).

As the pandemic began to unfold, scientific institutes and governments at different levels began to make data publicly available on the World Wide Web. Data collection protocols vary between institutions and over time. Additionally, few data sets include data for each of the compartments in a

SIR model. The New York Times’ “historical” data set¹ is an easily accessible source of data and is updated daily. These data comprise daily totals of “cases” and “deaths” for each county in the United States. I assume that the data included as “cases” are a reasonable approximations of the Infected compartment (I) in a SIR model. There are credible data of comparable scope on either the Susceptible or the Recovered compartments.

Model Structure

I make some simplifying assumptions in the face of incomplete data: (1) The entire population is susceptible so that $S/N = 1$. (2) Over the short term, the size of the Susceptible compartment does not change, $\frac{dS}{dt} = 0 = \frac{dN}{dt}$, eliminating the Susceptible compartment. (3) People who recover from a Covid-19 infection return to the Susceptible compartment, eliminating the Recovered compartment. With these assumptions, and with the addition of a “deaths” compartment, the simplified SIR model is

$$\frac{dI}{dt} = \beta I - \mu I - \gamma I \quad (5)$$

$$\frac{dD}{dt} = \mu I \quad (6)$$

Most importantly this model has state variables that might be matched to available observations.

The available data contain measurement errors of various types. Definitions and methods of detecting and reporting the numbers of infected persons and numbers of deaths attributable to Covid-19 have changed since

¹<https://github.com/nytimes/covid-19-data/>

January of 2020, are continuing to evolve, and can be expected to change in the future. Reporting protocols also vary between political jurisdictions (or “geographies” in the parlance of the New York Times). Finally, there is additional variability in the biosocial processes that mediate disease transmission.

State-space models separate variability in the biosocial processes in the system (transition model) from errors in observing features of interest in the system (observation model). (See Harvey 1990).

The general form of a state-space process or transition model is

$$\alpha_t = T(\alpha_{t-1}) + \Theta_t \quad (7)$$

where α_t is the state at time t and the function T embodies the dynamics mediating the development of the state at time t from the state at the previous time with random process error, Θ_t .

The transition model for the simplified SIR model is constructed from the explicit finite difference approximations of equations (5) and (6) with associated log-normal random errors.

$$I_t = I_{t-\Delta t} (1 + \Delta t (\beta_{t-\Delta t} - \mu_{t-\Delta t} - \gamma_{t-\Delta t})) e^{\eta_t} \quad (8)$$

$$D_t = (D_{t-\Delta t} + \Delta t \mu_{t-\Delta t} I_{t-\Delta t}) e^{\eta_t} \quad (9)$$

where η is a normal random deviate, $\eta \sim N(0, \sigma_\eta)$, representing temporal variability in the biosocial factors that mediate the spread of the pandemic. I have no particular justification, beyond the parsimony principle, for the assumption that the variance, σ_η , of the processes for I and D , should be the same.

The rate constants in the SIR model differential equations (in this case β , μ and γ) are often assumed to be invariant. This biological assumption clearly conflicts with the social assumptions that behavioral modification can reduce transmission rates and that medical advances can reduce both transmission and mortality rates. One approach to modeling time-dependent rates of transmission and mortality, β and μ , is to treat them as random effects (Skaug and Fournier 2006). Random effects are appropriate if repeating a time series of observations would not yield the same outcome as the initial observations. Random effects are also appropriate when observing the same process in two different areas. I model the β and μ time series as log-normal random walks. I assume that

$$\log \beta_t = \log \beta_{t-\Delta t} + \varepsilon; \quad \varepsilon \sim N(0, \sigma_\beta) \quad (10)$$

$$\log \mu_t = \log \mu_{t-\Delta t} + \varrho; \quad \varrho \sim N(0, \sigma_\mu) \quad (11)$$

A similar approach has been used by fisheries scientists to represent ill-determined parameters in fisheries stock assessment models, such as time-dependent fishing induced mortality (Nielsen and Berg 2014; Sibert 2017). The recovery rate, $\gamma_{t-\Delta t}$, in equation (8) is computed algebraically as

$$\gamma_{t-\Delta t} = \beta_{t-\Delta t} - \mu_{t-\Delta t} + \left(1 - \frac{I_t}{I_{t-\Delta t}}\right) \quad (12)$$

The general form of the state-space observation model is

$$x_t = O(\alpha_t) + \Omega_t \quad (13)$$

where the function O describes the measurement process with error Ω in observing the state α .

I applied separate observation error models for cases and deaths. The observation model for cases is a simple log-normal error

$$\log \varphi_t = \left(\log \frac{1}{\sqrt{2\pi\sigma_I^2}} - \left(\frac{\log I_t - \log \hat{I}_t}{\sigma_I} \right)^2 \right) \quad (14)$$

where I is the observed number of cases and \hat{I} is the number of cases predicted by equation (8).

Not all those afflicted by Covid-19 have died; there are far fewer deaths than infections. In addition, the observed time series for both I and D begins at the first recorded case, i.e. at time $t = 0$, $I_t \geq 1$. The first recorded death occurs several days or weeks after the first recorded case. Therefore the deaths time-series inevitably contains a substantial number of initial recorded zeros. The observation model for deaths accommodates observed zeroes by assuming to be “zero-inflated” log normal likelihood given by

$$\log \varepsilon_t = \begin{cases} D_t > 0 : & (1 - p_0) \cdot \left(\log \frac{1}{\sqrt{2\pi\sigma_D^2}} - \left(\frac{\log D_t - \log \hat{D}_t}{\sigma_D} \right)^2 \right) \\ D_t = 0 : & p_0 \cdot \log \frac{1}{\sqrt{2\pi\sigma_D^2}} \end{cases} \quad (15)$$

where D is the observed number of deaths, \hat{D} is the number of deaths predicted by equation 9, and p_0 is the proportion of observed deaths equal to zero.

Model parameters are estimated by maximizing the joint likelihood of the process errors, observation errors, and random effects.

$$L(\theta, \alpha, x) = \prod_{t=1}^m [\phi(\alpha_t - T(\alpha_{t-1}), \Theta)] \cdot \prod_{t=0}^m [\phi(x_t - O(\alpha_t), \Omega)] \quad (16)$$

where m is the number of days elapsed since the first recorded case, x_t is the vector of daily observations of cases and deaths, α_t is the vector of the daily

calculations of the state variables and random effects, and θ is a vector of model parameters (Table 1). The R package TMB (Kristensen et al. 2016) was used to estimate the parameters of the model. All R and C++ source files are available on github.²

Table 1: List of model variables for the simple SIR model, `simpleSIR4`. There are two state variables computed from the of estimated parameters and random effects. There are two random effects and five estimated variance parameters. All models variables are represented in the TMB C++ module as their natural logarithms.

Variable	Definition
<i>State variables:</i>	
I	Number of infected individuals
D	Number of deaths
<i>Random effects:</i>	
β_t	Transmission rate; log-normal random walk
μ_t	Mortality rate; log-normal random walk
<i>Estimated parameters:</i>	
σ_I	Infectious compartment estimation standard deviation
σ_D	Deaths compartment estimation standard deviation
σ_η	Standard deviation of transmission and deaths process errors
σ_β	Standard deviation of transmission rate random walk
σ_μ	Standard deviation of mortality rate random walk

Results

Six months after the pandemic began spreading in the United States, it was obvious that some areas were more successful than other in controlling the spread of the Covid-19 virus. Trends in the per-capita number of cases in the

²`simpleSIR4` at <https://github.com/johnrsibert/SIR-Models>

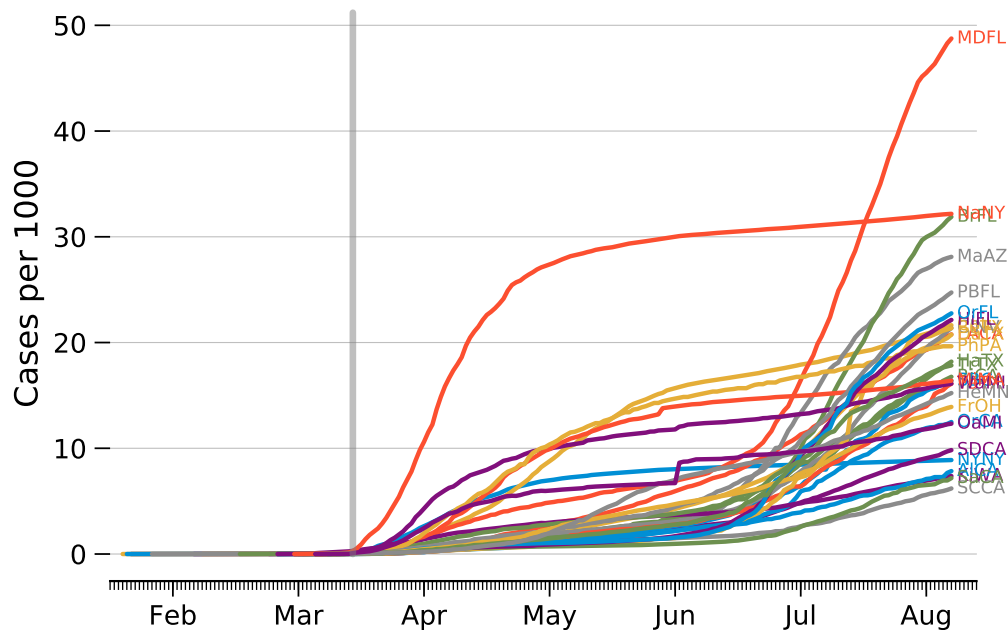


Figure 1: Trends in number of cases per 1000 people in the 30 most populous US counties. The vertical gray bar mark the March 19, 2020 California shelter in place order. See Table A.1 for key to county abbreviations.

thirty most populous counties in the United States are shown in Figure 1. These trends form a continuum from those that bend sharply upward, e.g. Miami-Dade Co. FL (MDFL), to those that appear to reach a plateau, e.g. Nassau Co. NY (NaNY).

Prevalence histories for counties representative of plateau and upward bending trajectories are shown in Figure 2. The 11-day moving averages of the daily increases in cases and deaths is a good indicator of the relative success in controlling the outbreak. The cumulative trends in number of

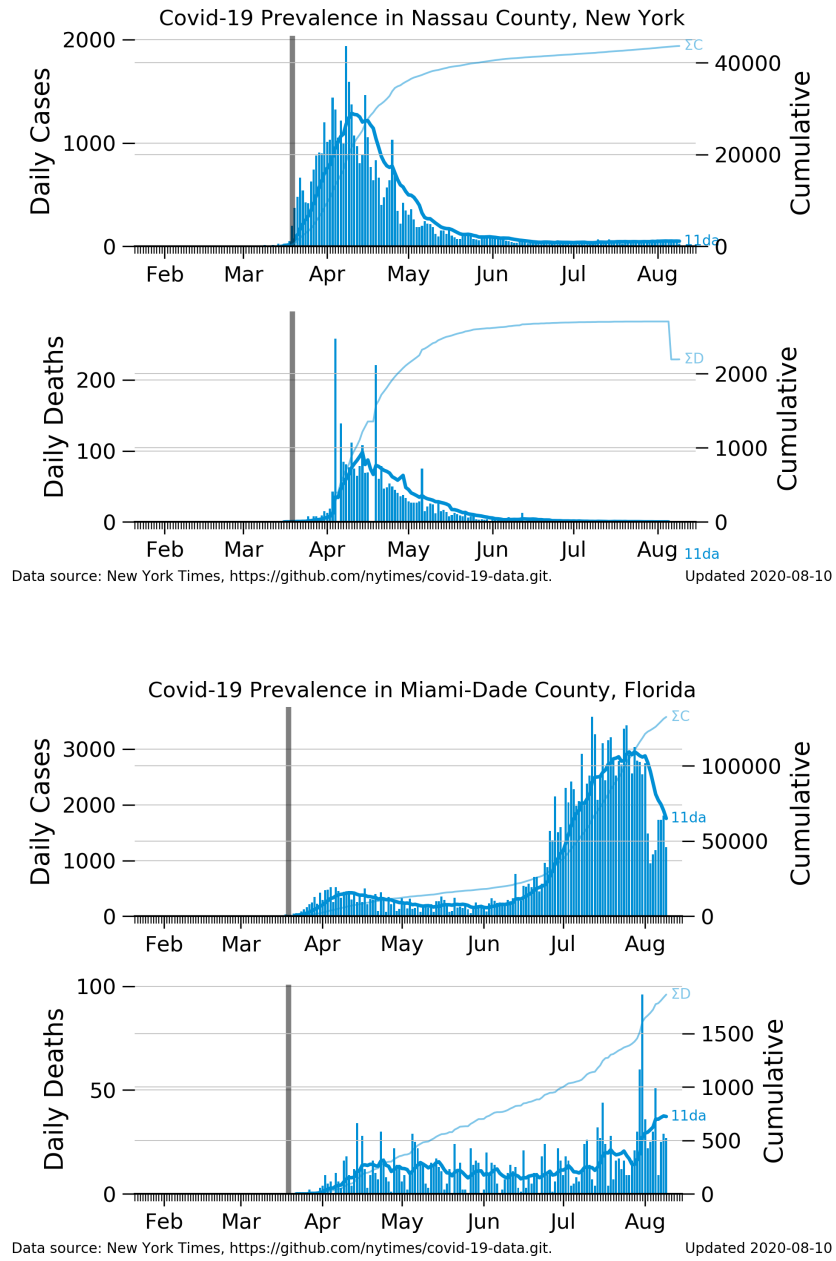


Figure 2: Prevalence trajectories for two US counties. Blue bars indicate daily increases increases in cases and deaths; dark blue lines enclosing the bars indicate 11 day moving averages of daily increases (labeled “11da”); pale blue lines indicate cumulative numbers of cases and deaths (labeled ΣC and ΣD); vertical gray bar marks the March 19, 2020 California shelter in place order.

cases is equivalent to the per capita trends in Figure 1. All histories show extreme day to day variability. Variability is most notable in the deaths time series, particularly for smaller counties.

The `simpleSIR4` model estimates two random effects and five parameters. In principle, all random effects and parameters are estimated simultaneously. Initial experiments with the model showed that several different numerical algorithms used to find the minimum of the log likelihood function were unable to reach a solution easily. Minima were reached for some counties, but most attempts terminated prematurely. Inspection of the diagnostic plots for the model showed that predicted values of cases and deaths matched observed values almost exactly with unrealistically low estimates of $\sigma_{\ln I}$ and $\sigma_{\ln D}$, figures C.3 and C.4 and table B.2.

The `simpleSIR4` model is easily configured with selected parameters fixed at constant values. All subsequent analysis focused on models with $\sigma_{\ln I} = 0.223$ and $\sigma_{\ln D} = 0.00953$. These standard deviations are equivalent to measurement errors of approximately 25% in reporting cases and 10% in reporting deaths. The algorithm converges to a solution in all cases, and converges rapidly using gradient methods.

Diagnostic indicators for the model estimates is plotted on logarithmic scales both to illustrate the lognormal likelihood functions used in the observation model, equations (14) and (15) and to illustrate trends in estimated transmission and mortality rates close to zero. The blue ‘+’ symbols represent the observed cases (I) and deaths (D). The red lines overlaying the symbols are model predictions (\hat{I}) and (\hat{D}) of cases and deaths. The shaded

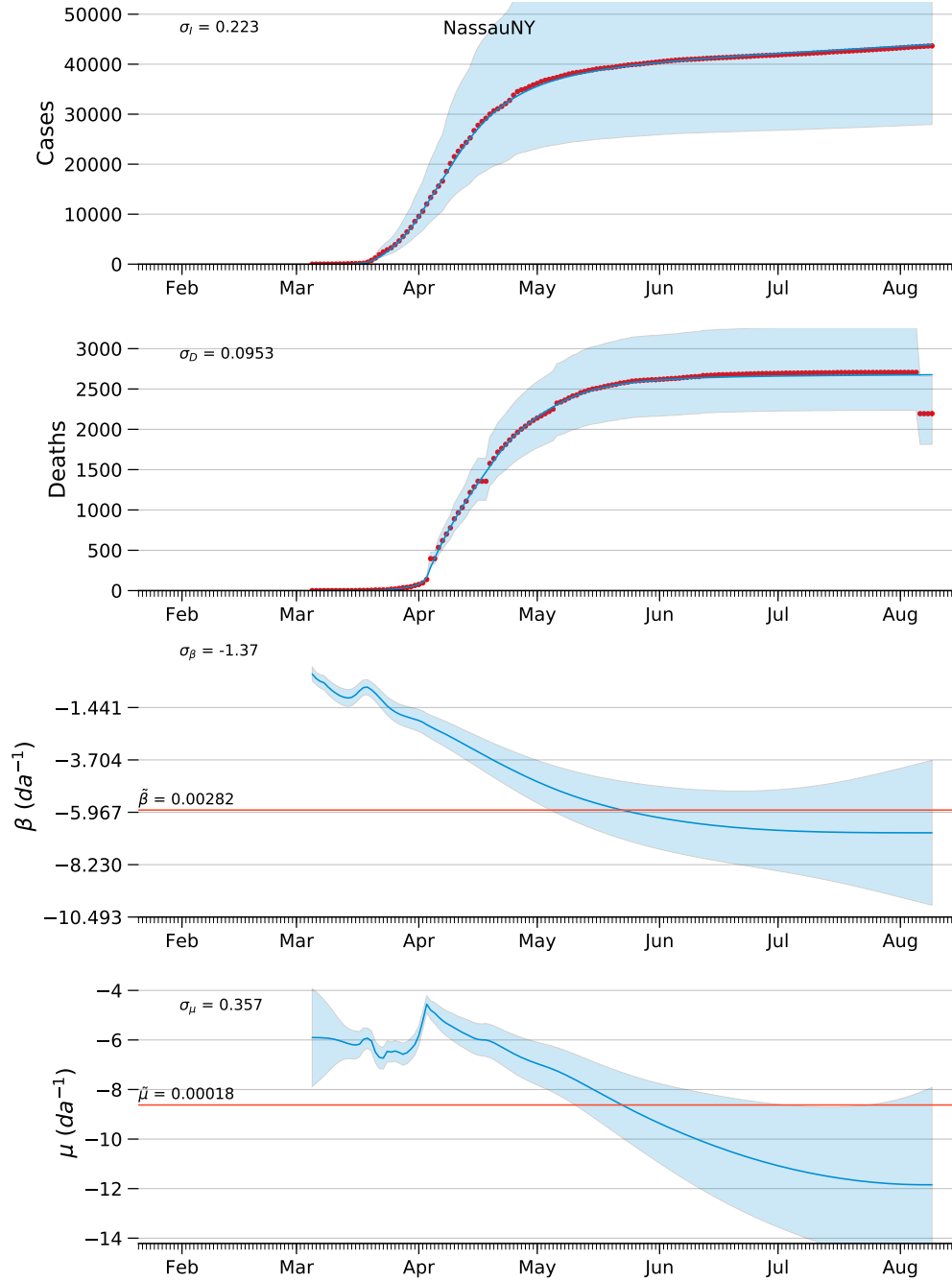


Figure 3: Diagnostic plots of model estimates for Nassau County, NY, with constraints of the observation model variance, $\sigma_{\ln I} = 0.223$ and $\sigma_{\ln D} = 0.00953$. See page 10 for explanation of figure.

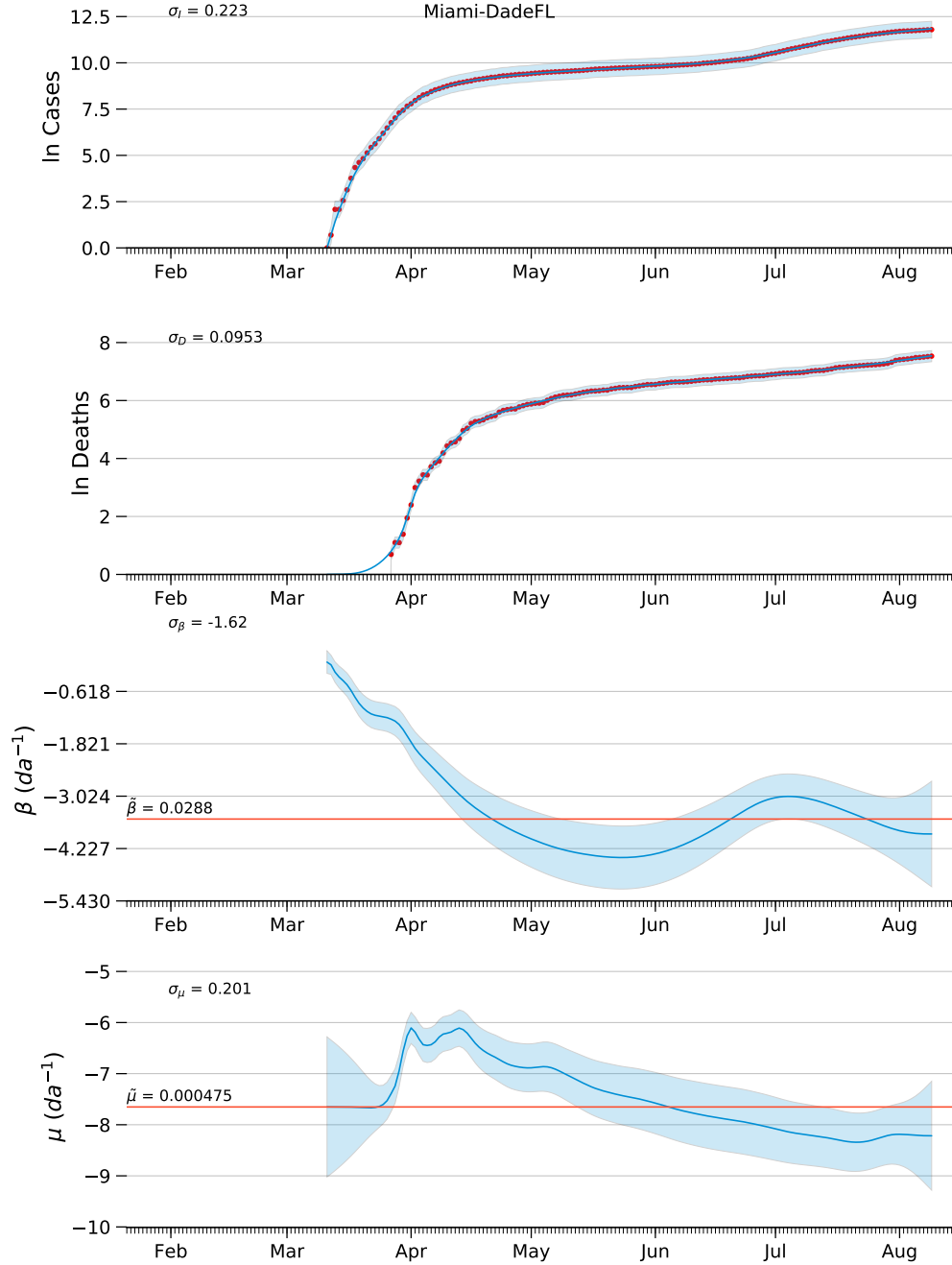


Figure 4: Diagnostic plots of model estimates for Miami-Dade County,FL, with constraints of the observation model variance, $\sigma_{\ln I} = 0.223$ and $\sigma_{\ln D} = 0.00953$. See page 10 for explanation of figure.

areas bounded by red outlines are ± 2 estimated standard deviations, $\sigma_{\ln I}$ and $\sigma_{\ln D}$ in the observation model, around the estimated trends. The solid blue lines in the transmission rate $\ln \beta$ and mortality rate $\ln \mu$ diagnostic plots are the estimated transmission and death rate random effects. The shaded areas bounded by blue outlines are estimated random effects ± 2 estimated standard errors of the random effect. The red lines labeled $\tilde{\beta}$ and $\tilde{\mu}$ are the medians of the estimated random effects over the time period.

Diagnostic plots for the constrained model are shown in figures 3 and 4 for convex downward and convex upward trajectories respectively. Estimated cases and deaths agree well with observation throughout the time series because of constraints on the observation model errors. Distinct trends in transmission rate estimates are plainly evident for the two prevalence patterns. A small, but distinct, transitory upward “bump” in July is evident for the convex downward example, Miami-Dade Co. FL. Estimated mortality rates trend generally downward for both patterns.

Figure 5 compares estimated transmission rate among counties. Transmission rates increased rapidly immediately after the first recorded case, and by early March the instantaneous transmission rate was greater than 1da^{-1} ($\ln \beta \approx 0$), equivalent to a doubling time of less than one day. Beginning in April, transmission rates fell substantially, and doubling times increased to longer than 20 days in some counties by late May. Counties with estimated transmission rates less than 0.007da^{-1} (or $\ln \beta \leq 5$) at the end of May correspond roughly to those counties with concave downward prevalence trajectories. Figure 6 is a simplified presentation of estimated transmission

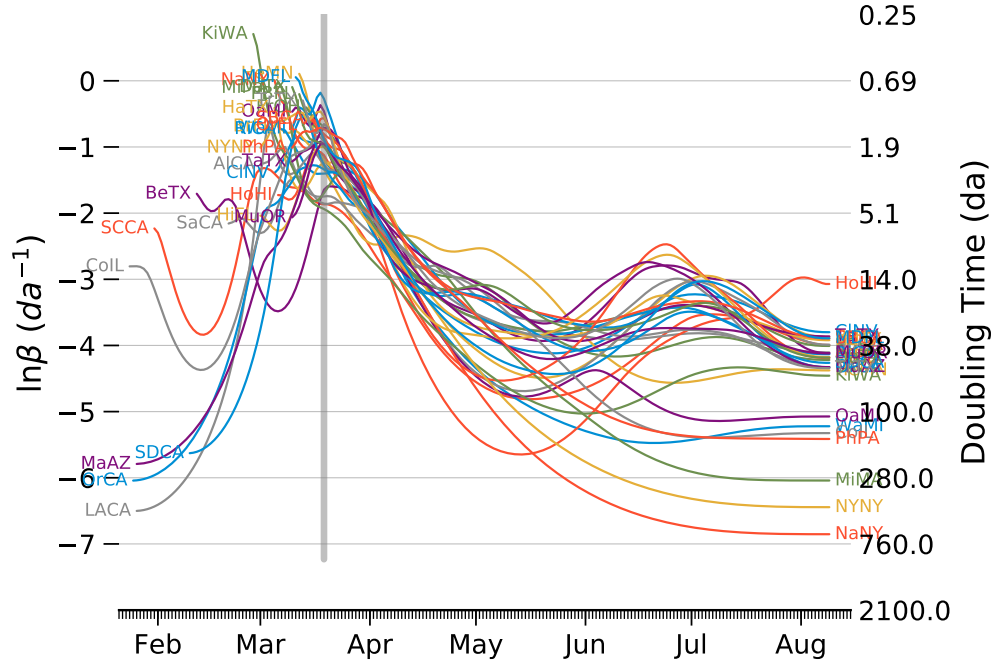


Figure 5: Estimated natural logarithms of the transmission rate for thirty two US counties using the constrained `simpleSIR4` model. Equivalent doubling times ($t_2 = \frac{\ln 2}{\exp(\ln \beta)}$) are shown on the right-hand ordinate. See Table A.1 for key to county abbreviations.

rate between counties that compare counties with sustainable suppression of transmission (Cook Co, IL, Nassau Co, NY) with two counties that have suffered a resurgence of cases (Honolulu Co, HI and Miami-Dade Co FL). The Honolulu example indicates that simply suppressing the transmission rate to a point where the doubling time is greater than 100 days does not ensure a sustainable outcome. The regions enclosed by ± 2 standard errors show that estimated transmission rates these four counties were similar in April and May, but diverged significantly in June to become distinct in August.

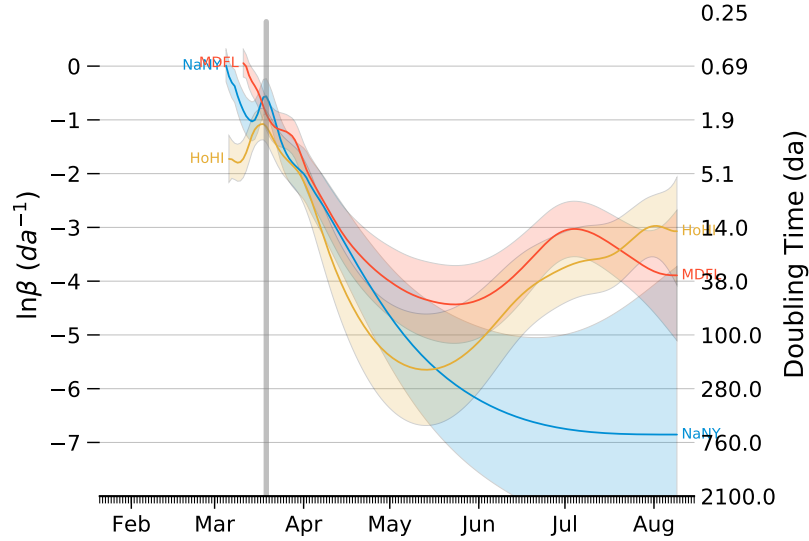


Figure 6: Estimated natural logarithms of the transmission rate for four US counties using the constrained `simpleSIR4` model. The shaded areas indicate the estimated random effect ± 2 estimated standard errors. Equivalent doubling times ($t_2 = \frac{\ln 2}{\exp(\ln \beta)}$) are shown on the right-hand ordinate. See Table A.1 for key to county abbreviations.

Figure 7 compares estimated mortality rate among counties. Initial mortality rates were quite variable during the first months of the pandemic and but rose quickly to around 0.01da^{-1} ($\ln \mu \approx 4.6$) in April. Subsequently the estimated mortality rates decreased similarly for all counties and appear to have leveled off in August to lows near 0.0003da^{-1} ($\ln \mu \approx -8$) in August.

Discussion

Nonlinear statistical models with multiple parameters rely on numerical methods to estimate parameters by searching for minima in the negative of the

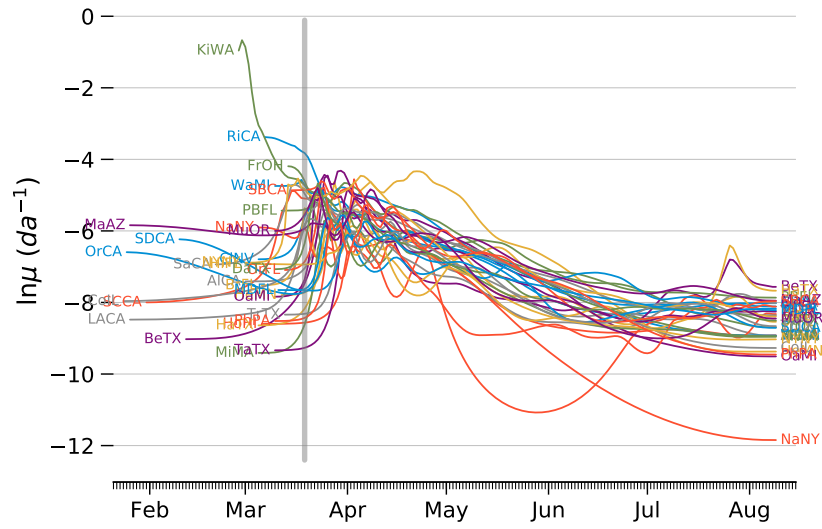


Figure 7: Estimated natural logarithms of the mortality rate for thirty two US counties using the constrained `simpleSIR4` model. See Table A.1 for key to county abbreviations.

likelihood function. The parameter values at the minima are considered to be maximum likelihood estimators. The minimization algorithms applied to unconstrained `simpleSIR4` do not reliably converge to solutions. The standard deviations in the observation model are components of the likelihood, and the algorithm pushes these parameters toward unrealistically low estimates. Setting the values of $\sigma_{\ln I}$ and $\sigma_{\ln D}$ to arbitrarily small constants allows the algorithm to estimate the other parameters.

The trends in estimated transmission rate Figure 5 seem reasonable. The extremely high transmission rates in March agree well with doubling times reported in newspaper articles at the time. The steady decline of transmission rates after shelter-in-place advice is also consistent with casual observation. The transmission rates estimated for several counties appear to trend upward, at least briefly, in July (figure 5). Counties that display this upward deflection are also counties that have not been successful in controlling spread of the outbreak

The incubation time of the Covid-19 virus is generally considered to be about 14 days (**Someone2020**). The trends in Figure 5 in conjunction with the observed trends suggest that sustainable containment of the pandemic does not occur unless the instantaneous transmission rate is forced below $0.018da^{-1}$, that is, unless the doubling time is greater than 35 days, approximately twice the incubation period.

The magnitude and variability of the mortality rate estimates (Figure 7) at the start of the time series may be a result of variable lags between between the first recorded case and the first recorded death. The first recorded death

in King Co. WA occurred on the second day of the time series when four cases were recorded. In contrast, the first recorded death in Middlesex Co. MA occurred on the sixteenth day of the time series when 177 cases were recorded.

References

- Baudin, Michale (2010). “Nelder-Mead User’s Manual”. In: April, p. 119.
- Chen, Yi-Cheng, Ping-En Lu, Cheng-Shang Chang, and Tzu-Hsuan Liu (2020). “A Time-dependent SIR model for COVID-19 with Undetectable Infected Persons”. In: pp. 1–18. arXiv: 2003.00122. URL: <http://arxiv.org/abs/2003.00122>.
- Harvey, A.C. (1990). *Forecasting, Structural Time Series Models and the Kalman Filter*. Cambridge: Cambridge University Press. ISBN: 978-0521321969.
- Kristensen, K., A. Nielsen, C.W. Berg, H.J. Skaug, and B.M. Bell (2016). “TMB: Automatic Differentiation and Laplace Approximation”. In: *Journal of Statistical Software* 70, pp. 1–21. DOI: [doi:10.18637/jss.v070.i05](https://doi.org/10.18637/jss.v070.i05).
- Nielsen, Anders and Casper W. Berg (2014). “Estimation of time-varying selectivity in stock assessments using state-space models”. In: *Fish. Res.* 158, pp. 96–101. ISSN: 01657836. DOI: [10.1016/j.fishres.2014.01.014](https://doi.org/10.1016/j.fishres.2014.01.014). URL: <http://dx.doi.org/10.1016/j.fishres.2014.01.014>.
- Roques, Lionel, Etienne Klein, Julien Papa, and Samuel Soubeyrand (2020). “Modele SIR mecanistico-statistique pour l’estimation du nombre d’infectes et du taux de mortalite par COVID-19”. In: pp. 1–11. arXiv: [arXiv: 2003.10720v2](https://arxiv.org/abs/2003.10720v2).
- Sibert, John (2017). “Assessing of a portion of the Pacific Thunnus albacares stock : Ahi in the Main Hawaiian Islands”. In: *arxiv.org* arXiv:1702. arXiv: [arXiv:1702.01217v1](https://arxiv.org/abs/1702.01217v1).
- Skaug, Hans J and David A Fournier (2006). “Automatic approximation of the marginal likelihood in non-Gaussian hierarchical models”. In: *Comput. Stat. Data Anal.* 51.2, pp. 699–709. ISSN: 01679473. DOI: [10.1016/j.csda.2006.03.005](https://doi.org/10.1016/j.csda.2006.03.005).

Appendices

A Abbreviation Key

Table A.1: Key to county name abbreviations.

Key	County	State	Key	County	State
AlCA	Alameda	CA	MuOR	Multnomah	OR
BeTX	Bexar	TX	NYNY	New York City	NY
BrFL	Broward	FL	NaNY	Nassau	NY
CINV	Clark	NV	OaMI	Oakland	MI
CoIL	Cook	IL	OrCA	Orange	CA
DaTX	Dallas	TX	OrFL	Orange	FL
FrOH	Franklin	OH	PBFL	Palm Beach	FL
HaTX	Harris	TX	PhPA	Philadelphia	PA
HeMN	Hennepin	MN	RiCA	Riverside	CA
HiFL	Hillsborough	FL	SBCA	San Bernardino	CA
HoHI	Honolulu	HI	SCCA	Santa Clara	CA
KiWA	King	WA	SDCA	San Diego	CA
LACA	Los Angeles	CA	SaCA	Sacramento	CA
MDFL	Miami-Dade	FL	TaTX	Tarrant	TX
MaAZ	Maricopa	AZ	TrTX	Travis	TX
MiMA	Middlesex	MA	WaMI	Wayne	MI

B Estimation results

Table B.1: Model results. Estimating β and μ trends as random effects with constraints on σ_I and σ_D . Counties sorted in order of decreasing transmission rate (β). Data updated 2020-08-04 from <https://github.com/nytimes/covid-19-data.git>.2020-08-04

County	n	p_0	f	C	σ_η	σ_β	σ_μ	σ_I	σ_D	$\tilde{\gamma}$	$\tilde{\beta}$	$\tilde{\mu}$
Nassau, NY	151	0.0789	-348	0	0.14	0.256	0.346	0.223	0.0953	-1.22e-08	0.00322	0.000241
New York City, NY	155	0.0833	-310	0	0.161	0.217	0.36	0.223	0.0953	-2.36e-08	0.00533	0.000405
Wayne, MI	146	0.0544	-336	0	0.14	0.229	0.16	0.223	0.0953	-1.8e-08	0.00619	0.000875
Oakland, MI	146	0.068	-332	0	0.137	0.226	0.426	0.223	0.0953	-1.62e-08	0.0101	0.000594
Philadelphia, PA	146	0.102	-340	0	0.126	0.175	0.425	0.223	0.0953	-2.42e-08	0.0106	0.000532
Middlesex, MA	151	0.105	-357	0	0.124	0.237	0.371	0.223	0.0953	-1.25e-08	0.0107	0.000451
King, WA	157	0.0633	-431	0	0.126	0.234	0.339	0.223	0.0953	-8.63e-09	0.013	0.000481
Franklin, OH	142	0.0629	-419	0	0.102	0.157	0.3	0.223	0.0953	-1.76e-08	0.0208	0.00101
Honolulu, HI	150	0.166	-484	0	0.0721	0.227	0.49	0.223	0.0953	-5.15e-08	0.0215	0.000174
Cook, IL	192	0.275	-473	0	0.101	0.234	0.217	0.223	0.0953	-2.2e-07	0.0226	0.000466
Alameda, CA	155	0.141	-465	0	0.0808	0.133	0.248	0.223	0.0953	-3.45e-08	0.0231	0.000527
Multnomah, OR	146	0.0272	-497	0	0.0798	0.181	0.318	0.223	0.0953	-5.07e-08	0.0233	0.000362
Santa Clara, CA	185	0.204	-586	0	0.071	0.237	0.274	0.223	0.0953	-1.55e-07	0.0246	0.000352
Los Angeles, CA	190	0.236	-454	0	0.102	0.305	0.244	0.223	0.0953	-3.45e-07	0.0249	0.000423
San Diego, CA	175	0.244	-430	0	0.0956	0.277	0.317	0.223	0.0953	-2.63e-07	0.0267	0.000719
Riverside, CA	149	0.06	-482	0	0.09	0.138	0.183	0.223	0.0953	-2.72e-08	0.0294	0.000895
Palm Beach, FL	144	0.069	-378	0	0.111	0.166	0.157	0.223	0.0953	-1.54e-08	0.0302	0.000942
Harris, TX	151	0.0921	-373	0	0.102	0.197	0.322	0.223	0.0953	-2.44e-08	0.0302	0.000301
Miami-Dade, FL	145	0.11	-342	0	0.133	0.197	0.206	0.223	0.0953	-1.08e-08	0.0308	0.000473
Orange, FL	143	0.0208	-418	0	0.101	0.21	0.435	0.223	0.0953	-1.98e-08	0.0314	0.00024
Clark, NV	151	0.0724	-436	0	0.1	0.158	0.218	0.223	0.0953	-3.3e-08	0.0319	0.000743
Travis, TX	143	0.0972	-359	0	0.1	0.19	0.271	0.223	0.0953	-1.73e-08	0.0327	0.000319
Tarrant, TX	146	0.068	-414	0	0.1	0.138	0.42	0.223	0.0953	-3.12e-08	0.0328	0.000335
Broward, FL	150	0.0728	-391	0	0.107	0.167	0.447	0.223	0.0953	-2.15e-08	0.0333	0.000411
Orange, CA	191	0.313	-519	0	0.0769	0.234	0.266	0.223	0.0953	-3.73e-07	0.0334	0.000732
Dallas, TX	146	0.0612	-388	0	0.11	0.17	0.309	0.223	0.0953	-1.43e-08	0.0336	0.000504
San Bernardino, CA	141	0.0634	-406	0	0.0999	0.14	0.198	0.223	0.0953	-2.06e-08	0.0343	0.000794
Sacramento, CA	164	0.109	-574	0	0.0666	0.174	0.252	0.223	0.0953	-8.02e-08	0.0343	0.000428
Hennepin, MN	144	0.103	-359	0	0.114	0.207	0.402	0.223	0.0953	-1.24e-08	0.036	0.000917
Hillsborough, FL	155	0.16	-461	0	0.0813	0.189	0.227	0.223	0.0953	-7.15e-08	0.0373	0.00065
Maricopa, AZ	190	0.283	-482	0	0.0897	0.235	0.158	0.223	0.0953	-4e-07	0.0422	0.00188
Bexar, TX	173	0.224	-478	0	0.0745	0.213	0.376	0.223	0.0953	-7.61e-08	0.0461	0.000393
Median	150.5	0.09465	-418.5	0	0.101	0.202	0.3045	0.223	0.0953	-2.43e-08	0.0298	0.000477

Table B.2: Model results. Estimating β and μ trends as random effects without constraints on σ_I and σ_D . Counties sorted in order of decreasing transmission rate (β). Data updated 2020-08-04 from <https://github.com/nytimes/covid-19-data.git>. 2020-08-04

County	n	p_0	f	C	σ_η	σ_β	σ_μ	σ_I	σ_D	$\tilde{\gamma}$	β	$\tilde{\mu}$
Nassau, NY	151	0.0789	-1190	1	0.231	0.603	10.3	0.000183	3.29e-08	-9.46e-09	0.00295	9.88e-05
New York City, NY	155	0.0833	-1000	0	0.187	1.04	1.01	0.000436	0.000367	-2.73e-08	0.00476	0.000234
Oakland, MI	146	0.068	-836	1	0.16	1.55	1.18	9.12e-07	0.00426	-1.91e-08	0.00669	0.000318
Cook, IL	192	0.275	-1100	1	0.116	3.68	0.992	8.16e-08	8.01e-05	-2.24e-07	0.00679	0.000201
Wayne, MI	146	0.0544	-856	1	0.192	1.15	1.46	0.000795	0.000936	-2.57e-08	0.00701	0.000362
Philadelphia, PA	146	0.102	-728	1	0.159	1	1.98	0.00274	0.00396	-3.1e-08	0.00964	0.000227
Middlesex, MA	151	0.105	-836	0	0.162	1.05	1.24	0.000663	0.00204	-1.56e-08	0.00995	0.000331
King, WA	157	0.00633	-1080	1	0.147	0.474	0.909	0.00206	0.00224	-5.99e-09	0.0133	0.000455
Honolulu, HI	150	0.166	-1480	10	0.116	4.87	117	0.000734	3.7e-06	-5.53e-08	0.0156	1.46e-11
Santa Clara, CA	185	0.204	-1280	1	0.104	4.78	7.43	9.33e-08	2.29e-06	-1.53e-07	0.0158	1.16e-07
Sacramento, CA	164	0.109	-803	10	0.123	3.17	2.46	1.44e-06	0.0049	-8.81e-08	0.0183	0.00016
Multnomah, OR	146	0.0272	-894	1	0.119	0.896	3.35	0.0036	0.00226	-6.79e-08	0.0234	5.44e-05
Franklin, OH	142	0.0629	-819	1	0.123	0.462	1.3	0.00255	0.00368	-1.42e-08	0.0239	0.000575
Los Angeles, CA	190	0.236	-971	1	0.242	0.889	0.983	2.22e-06	0.00661	-3.77e-07	0.024	0.000399
Alameda, CA	155	0.141	-905	1	0.131	3.61	20.3	2.65e-05	6.68e-08	-3.95e-08	0.0241	9.44e-10
San Diego, CA	175	0.244	-850	1	0.161	1.08	1.23	4.71e-06	0.0103	-2.91e-07	0.0247	0.000335
Bexar, TX	173	0.224	-689	1	0.131	2.61	1.44	0.000397	0.0103	-7.18e-08	0.0261	0.000256
Orange, CA	191	0.313	-878	1	0.127	1.54	0.961	6.16e-06	0.053	-4.02e-07	0.0268	0.000509
Orange, FL	143	0.0208	-710	1	0.119	0.678	1.08	0.0015	0.0373	-2.3e-08	0.027	0.000192
Clark, NV	151	0.0724	-662	10	0.148	1.5	5.31	0.00247	1.25e-05	-4.16e-08	0.0276	0.000322
Tarrant, TX	146	0.068	-662	1	0.14	1.24	1.34	0.00891	0.00326	-3.79e-08	0.0283	0.000269
Harris, TX	151	0.0921	-429	1	0.116	0.27	0.965	0.156	0.0215	-2.11e-08	0.0297	0.000289
Palm Beach, FL	144	0.069	-507	0	0.137	0.337	1.31	0.0822	0.00588	-1.16e-08	0.0302	0.000525
San Bernardino, CA	141	0.0634	-567	1	0.146	1.74	2.74	0.0051	0.00586	-1.74e-08	0.0304	0.000207
Miami-Dade, FL	145	0.11	-722	10	0.156	0.639	0.961	6.89e-06	0.00814	-9.55e-09	0.0313	0.000447
Hennepin, MN	144	0.103	-726	0	0.14	0.72	1.35	0.00522	0.00203	-9.13e-09	0.0314	0.00048
Riverside, CA	149	0.06	-683	1	0.113	1.25	5.23	0.0174	2.17e-05	-2.61e-08	0.0317	0.000718
Maricopa, AZ	190	0.283	-932	1	0.105	1.23	1.26	5.43e-06	0.0164	-4.2e-07	0.0322	0.000596
Travis, TX	143	0.0972	-394	1	0.14	1.07	1.44	0.177	0.0131	-1.67e-08	0.0329	0.000265
Hillsborough, FL	155	0.16	-653	0	0.111	1.11	1.28	0.00477	0.0169	-7.24e-08	0.0329	0.000393
Broward, FL	150	0.0728	-584	1	0.13	0.23	1.63	0.0759	0.00289	-2.03e-08	0.0331	0.000275
Dallas, TX	146	0.0612	-529	1	0.13	0.303	1.26	0.0757	0.00757	-1.04e-08	0.0349	0.000342
Median	150.5	0.09465	-811	1	0.134	1.065	1.325	0.0011475	0.00382	-2.67e-08	0.0254	0.0003035

C Diagnostic Plots

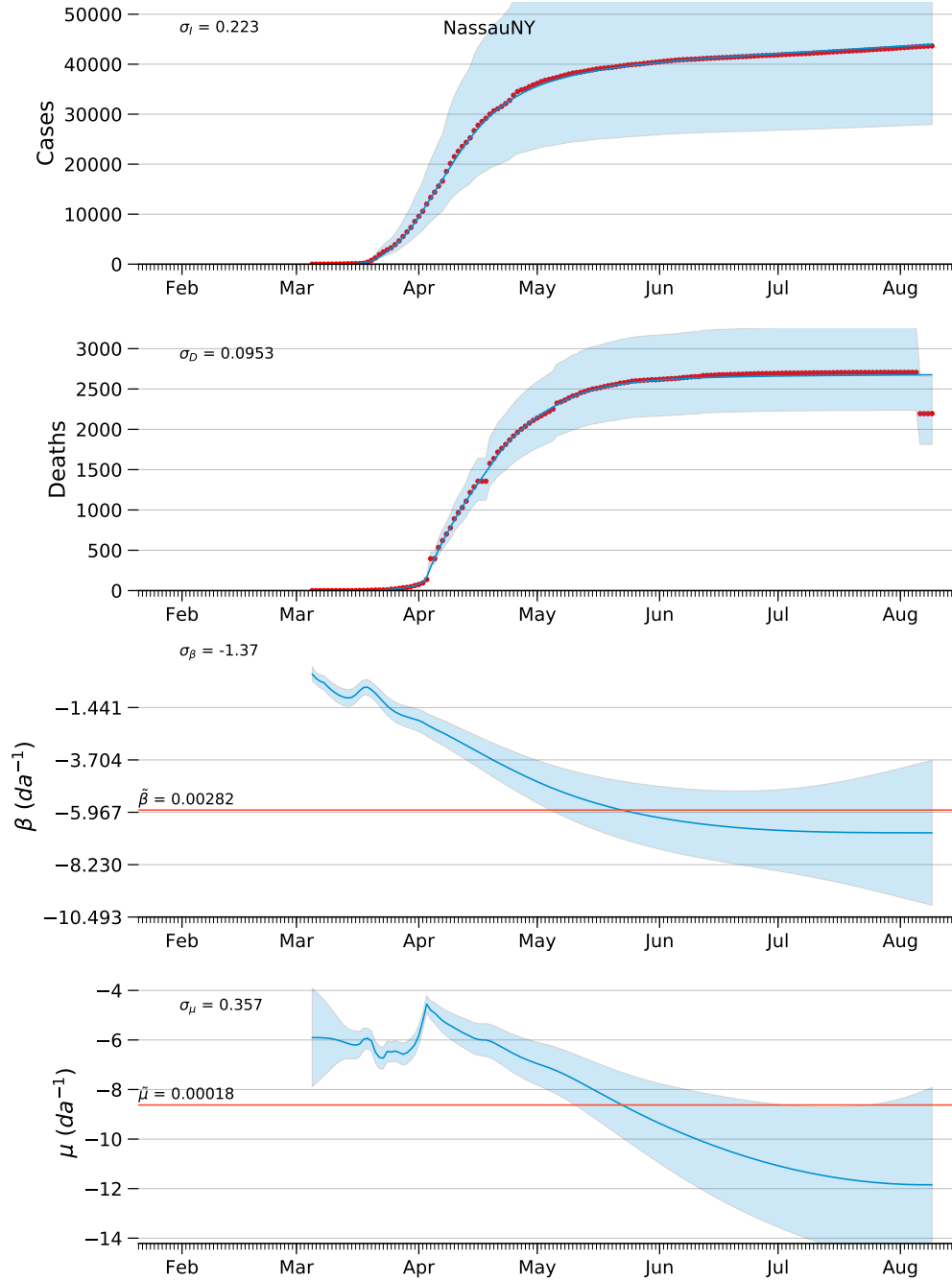


Figure C.1: Diagnostic plots of model estimates for Nassau County, NY, with constraints of the observation model variance, $\sigma_{\ln I} = 0.223$ and $\sigma_{\ln D} = 0.00953$. Cases and deaths plotted on arithmetic scale. See page 10 for explanation of figure.

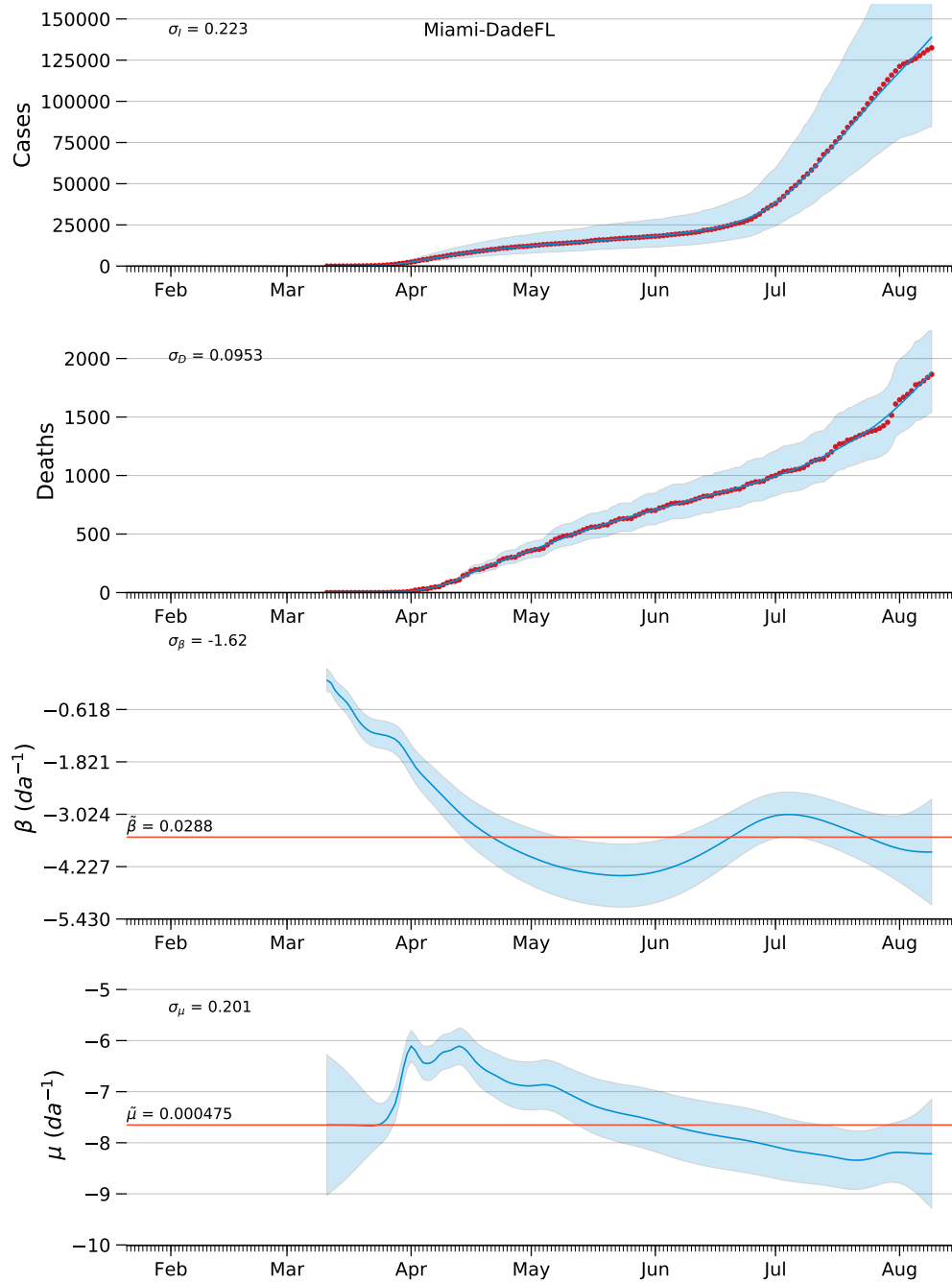


Figure C.2: Diagnostic plots of model estimates for Miami-Dade County, FL with constraints of the observation model variance, $\sigma_{\ln I} = 0.223$ and $\sigma_{\ln D} = 0.00953$. Cases and deaths plotted on arithmetic scale. See page 10 for explanation of figure.

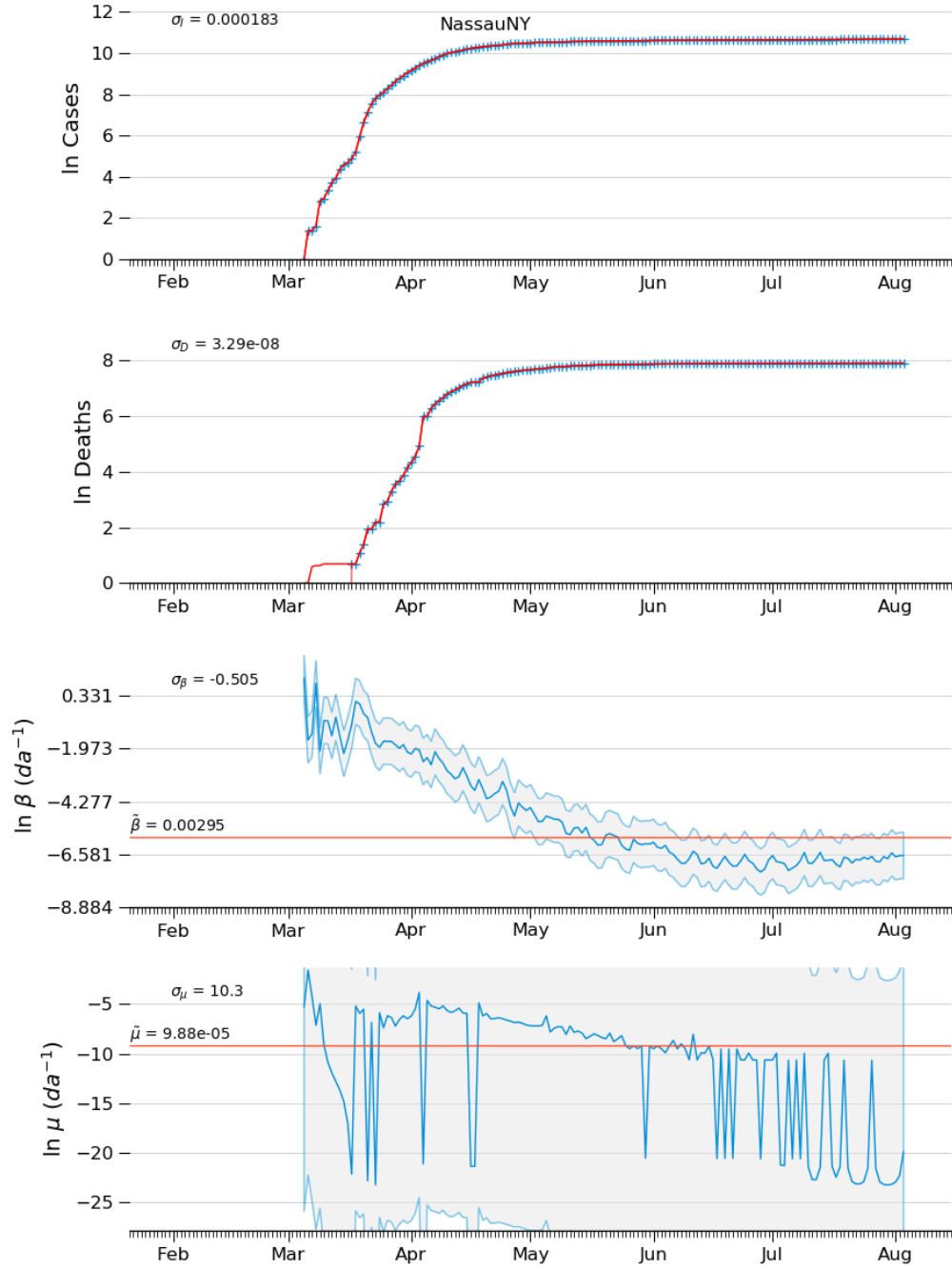


Figure C.3: Diagnostic plots of model estimates for Nassau County, NY, without constraints of the observation model variance. See page 10 for explanation of figure.

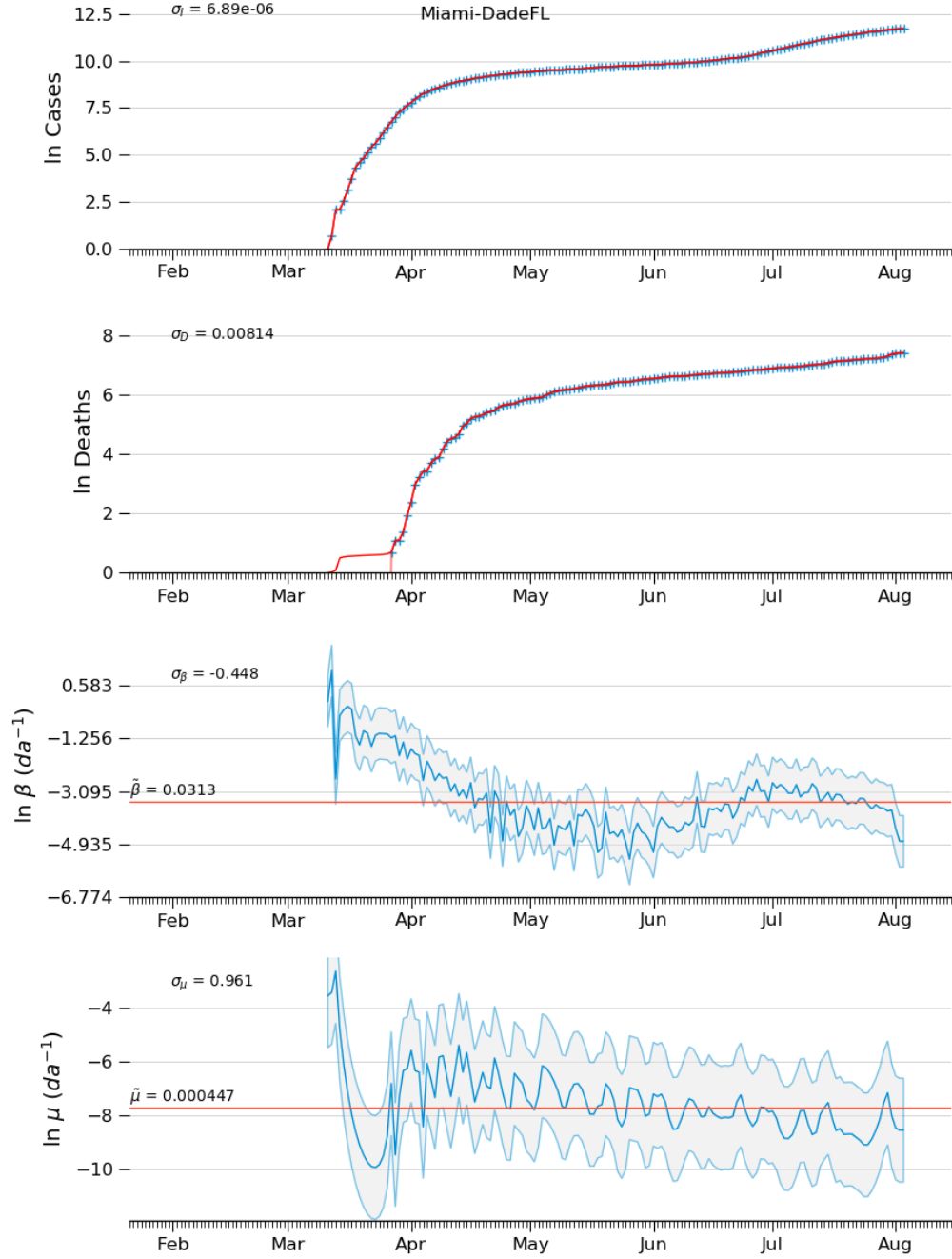


Figure C.4: Diagnostic plots of model estimates for Miami-Dade County,FL, without constraints of the observation model variance. See page 10 for explanation of figure.